

## A RANS modelling approach for predicting powering performance of ships in waves

Björn Windén<sup>1</sup>, Stephen Turnock<sup>1</sup> and Dominic Hudson<sup>1</sup>

<sup>1</sup>*Fluid Structure Interactions Research Group University of Southampton, Southampton, United Kingdom.*

**ABSTRACT:** *In this paper, a modelling technique for simulating self-propelled ships in waves is presented. The flow is modelled using a RANS solver coupled with an actuator disk model for the propeller. The motion of the ship is taken into consideration in the definition of the actuator disk region as well as the advance ratio of the propeller. The RPM of the propeller is controlled using a PID-controller with constraints added on the maximum permissible RPM increase rate. Results are presented for a freely surging model in regular waves with different constraints put on the PID-controller. The described method shows promising results and allows for the studying of several factors relating to self-propulsion. However, more validation data is needed to judge the accuracy of the model.*

**KEY WORDS:** RANS, Self-propulsion, Waves, Body force, Actuator disk, Control, RPM limiting

### INTRODUCTION

The performance of a ship when travelling in a seaway has always been a hot topic. This is true now more than ever with ever increasing requirements for environmental performance and rapid transit of goods. The introduction of the Energy Efficiency Design Index (EEDI) as a design constraint for new ships from 2013 (IMO, 2011) is likely to lead to an increased need for design modifications that lead to improved efficiency without negatively impacting other factors such as transport capacity, safety, etc. Accurately predicting performance in waves and being able to judge the impact of subtle design changes is therefore identified as an area of high interest. From a hydrodynamical point of view, understanding the interaction between the ship, the sea state that it is in and the propeller that is powering it will give an answer to most questions regarding performance. A schematic of this interaction created by Windén (2012) is shown in Fig. 1.

To properly model this interaction, strong linking is needed between flow conditions around the hull and the performance of the propeller. Currently, the only method that allows for detailed flow features around the hull and the propeller to be modelled is a Navier-Stokes (NS) based solver.

---

Corresponding author: Björn Windén, e-mail: [b.winden@soton.ac.uk](mailto:b.winden@soton.ac.uk)

This is an Open-Access article distributed under the terms of the Creative Commons Attribution Non-Commercial License (<http://creativecommons.org/licenses/by-nc/3.0>) which permits unrestricted non-commercial use, distribution, and reproduction in any medium, provided the original work is properly cited.

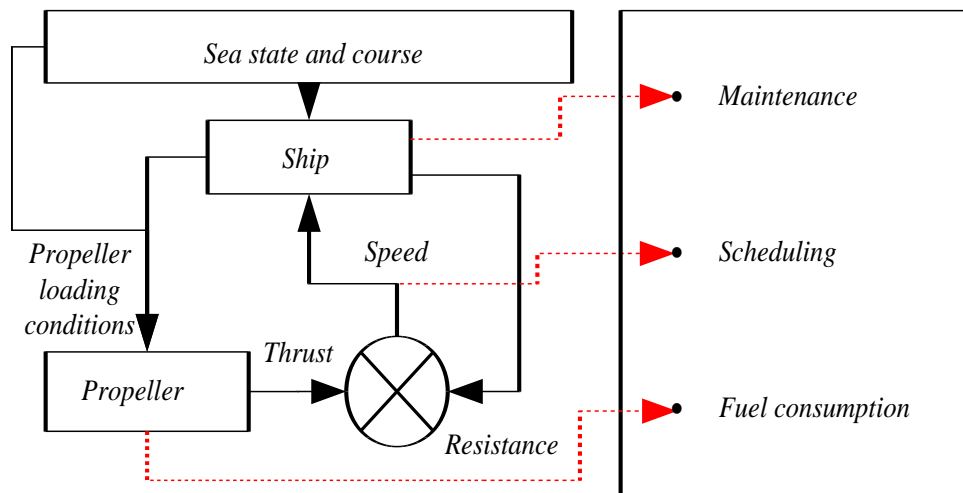


Fig. 1 Hydrodynamics related to performance in waves.

## APPROACH

One reason why proper verification and validation of NS based modelling of ships in waves is hard to achieve is the complexity of the model itself. For self-propulsion, a way to model the rotating propeller has to be added on top of the already complex dynamical geometry. This leads to a difficulty in identifying the most important sources of error. For example incorrect phasing of forces and motions has been identified as a problem in recent workshops (Larsson et al., 2014). If the motions are seen to be out of phase, it is hard to tell if this is due to incorrect forcing, a problem with the mesh deformation scheme or the coupling scheme between forces and motions. This means that the predicted propulsive performance of the ship has many associated error sources and it may be hard to clearly quantify the underlying reason for the error.

One of the most well adopted ways to address a problem with many unknowns is to start with something that is known or can be found out easily and gradually build understanding from this. Applying this reasoning to the problem of modelling ship performance in waves means removing many of the uncertainties mentioned above. RANS is chosen as a modelling technique due to its advantage in computational efficiency over other NS based methods. A validation study based on experiments by Journée (1992) of the forces and moments on a fixed Wigley hull in waves predicted using the open source CFD software OpenFOAM has been carried out by Windén et al. (2012). Fig. 2 shows encouraging results for the prediction of the amplitude of the forces at different wavelengths but a problem with the phasing still remains even when the hull is fixed. The study also compares results with a nonlinear Boundary Element Method (BEM) by Kjellberg (2011) which seemed to predict the phasing slightly better while giving a greater error in predicting the amplitudes of the forces.

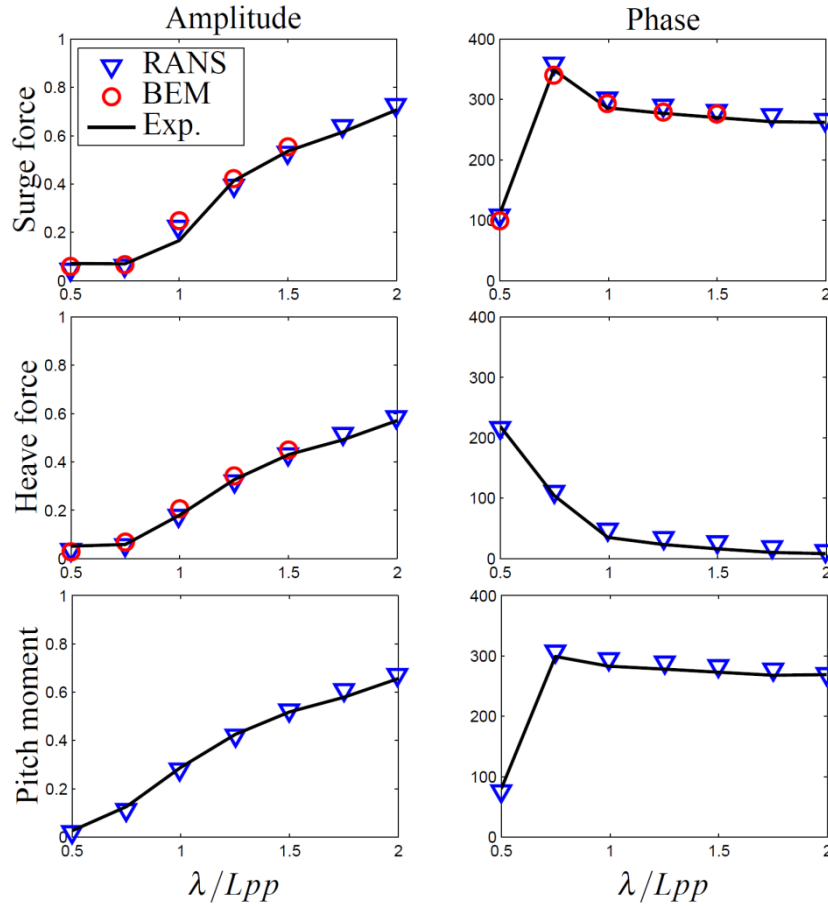


Fig. 2 Results of validation case.

The next step after the forces and moments are validated is either to study the motions or to study propulsion. In this paper, the second issue is addressed. The objective is to identify more about what factors should be considered when modelling self-propelled ships in waves using RANS. In the simulations in this paper, the model is free to surge and the RPM of the propeller is controlled using a PID-controller. This means that the influence of the propeller thrust on the surge for different control conditions can be studied.

## GEOMETRY AND MESHING

The setup of the numerical towing tank is shown in Fig. 3. The size of the computational domain is set so that  $L_f = L$  and  $L_a = 4L$ . Waves are generated and dissipated using the relaxation-based wave generation toolbox waves2Foam (Jacobsen et al., 2012). The relaxation zones are designed so that  $L_g = L_d = 2\lambda$ . Forward speed is modelled using a steady current which is set corresponding to  $Fn = 0.2$ . The waves are chosen to have an amplitude of  $\zeta = 0.023m$  which corresponds to about 12% of the model draught. The wavelength is set to be equal to the model length so that  $\lambda = L$ .

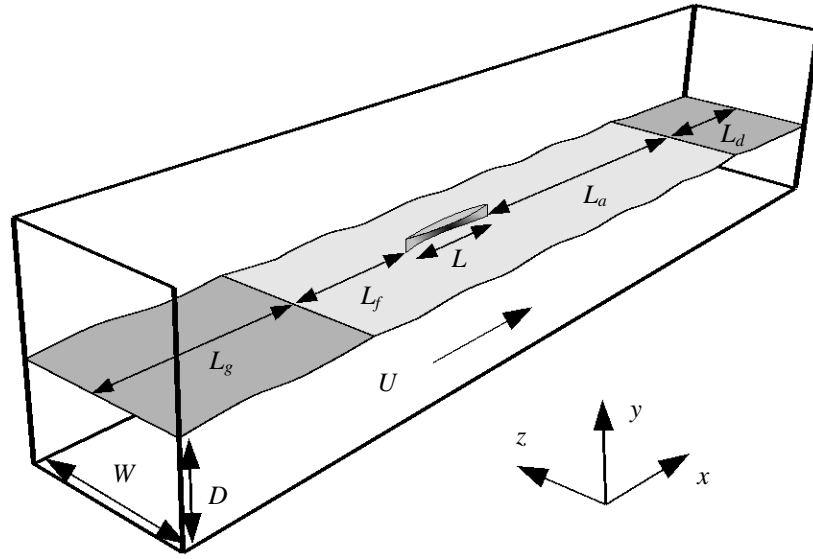


Fig. 3 Geometry of the numerical towing tank.

The mesh is created using an automated refinement strategy described by Windén et al. (2012). The final mesh size lies around 6M cells with a  $y^+$  value of around 2. The mesh is designed to ensure

- an adequate distribution of cells in the free surface region
- adequate refinement around the hull, in the wake and in the propeller region
- smooth blending between the refinement in these two areas where they intersect

The particulars of the chosen hull are shown in Table 1.

Table 1 Particulars of tested hulls.

$L$	$3m$	$B$	$0.3m$	$a_2$	$0.2$
$T$	$0.1875m$	$\nabla$	$0.0780m^2$		

where  $a_2$  gives the shape of the hull as

$$z = \frac{B}{2} \left[ 1 - \left( \frac{y}{T} \right)^2 \right] \left[ 1 - \left( \frac{2x}{L} \right)^2 \right] \left[ 1 + a_2 \left( \frac{2x}{L} \right)^2 \right] \quad (1)$$

## PROPELLER MODELLING

The Wigley hull is a purely academical hullform and has no consideration of propeller positioning in the definition of its shape. The propeller disc is therefore positioned half a radius behind the aft perpendicular, with a lower point flush with the keel and with a diameter of 85% of the draught. This is seen as representative of a typical positioning of the propeller on a ship. The positioning of the propeller disc relative to the rear profile of the used Wigley hull is shown in Fig. 4. Furthermore a hub with a radius of 10% of the total disk radius is used as well as a shaft extending into the hull and ending in an ellipsoid cap to minimise separation.

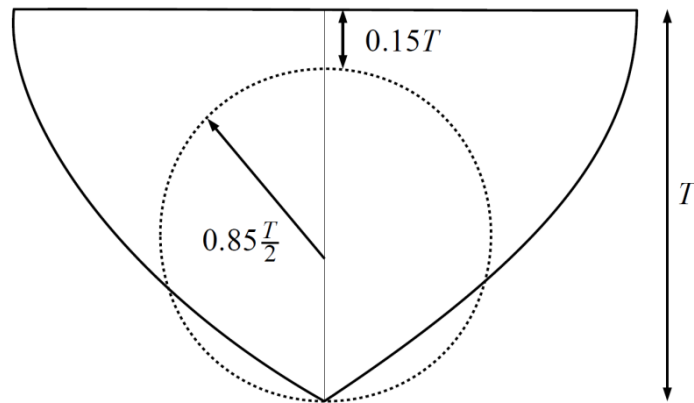


Fig. 4 Positioning of propeller disc behind Wigley hull.

The propeller is modelled using a body force approach, meaning that an external force is added to the RANS momentum equation to represent the work done on the fluid by the propeller. The body force due to the propeller  $F_v$  is defined as a force per unit volume and is incorporated in the momentum equation as

$$\frac{\partial \bar{u}_i}{\partial t} + \bar{u}_j \frac{\partial \bar{u}_i}{\partial x_j} = \frac{1}{\rho} \left( \mu \frac{\partial^2 \bar{u}_i}{\partial x_j^2} - \frac{\partial \tau_{ij}}{\partial x_i} + \frac{\partial \bar{p}}{\partial x_i} + F_v \right) \quad (2)$$

In Equation 2, the left hand side represents the momentum change of the fluid. The average velocity components are denoted as  $u_i$  with  $i = 1, 2, 3$ . The right hand side of Equation 2 represents stresses where the body force vector  $F_v$  is added to the pressure gradient, the viscous stresses and the Reynolds stress tensor  $\tau_{ij}$  which is modelled using the turbulence model  $k - \omega$  SST (Menter et al., 2003).

### Active cell identification

The magnitude and direction of  $F_v$  in every cell in the domain is decided by the location of that cell in relation to the propeller to be modelled. Cells within the propeller disk will be active (i.e. be eligible to receive an  $F_v > 0$ ). To not perform unnecessary calculations, these cells must be identified before any body force is added. Firstly, the centroid of the propeller in the undisturbed state is denoted  $x_{p_0}$ , the initial centre of gravity of the hull  $CG_0$  and the orientation of the propeller axis in relation to the initial state  $O_0$ . An arbitrary rotation and translation of the initial state is shown in Fig. 5. The rotation tensor due to the rotation of the hull in three degrees of freedom (pitch, roll and yaw) is denoted as  $Q$  so that

$$Global\ vector = Q \cdot Local\ vector \quad (3)$$

and the planar shift of the centre of gravity due to motions is denoted  $P$ . With this notation, the location of the propeller centroid  $x_p$  at an arbitrary position and orientation of the hull is

$$x_p = CG_0 + P + Q \cdot (x_{p_0} - CG_0) \quad (4)$$

and the orientation of the propeller axis  $O$  (normal to the propeller disk plane) is

$$O = Q \cdot O_0 \quad (5)$$

A cell is given a non-zero value of  $F_v$  if it lies within the radius of the propeller disk  $R$  but outside of the hub radius  $R_H$  and within the thickness of the disk  $d$ . A vector  $v_I$  is defined as going between the current propeller centroid  $x_p$  and the centre of cell  $I$ . The distance from the propeller centroid along the propeller normal axis ( $|d_I|$ ) is found from

$$d_I = O(v_I \cdot O) \quad (6)$$

The local radius of cell  $I$ ,  $R_I$  is found by projecting the vector  $v_I$  onto the propeller plane. Since the normal vector to the propeller plane is the vector  $O = (O_1, O_2, O_3)$ , the projection of  $v_I$  onto the propeller plane is achieved by

$$R_I = \begin{bmatrix} O_2^2 + O_3^2 & -O_1 O_2 & -O_1 O_3 \\ -O_1 O_2 & O_1^2 + O_3^2 & -O_2 O_3 \\ -O_1 O_3 & O_2 O_3 & O_1^2 + O_2^2 \end{bmatrix} v_I \quad (7)$$

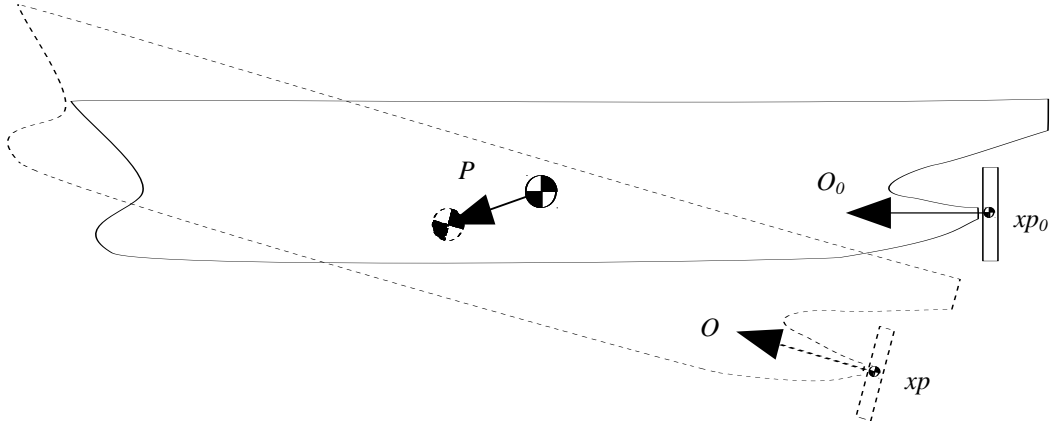


Fig. 5 Arbitrary rotation and translation of initial state.

The definitions of  $R_I$ ,  $d_I$  and  $v_I$  are shown in Fig. 6

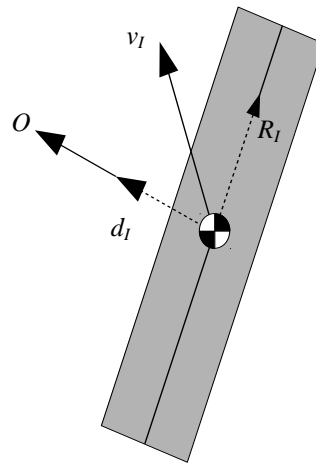


Fig. 6 Definitions of propeller disk extent.

From this definition it follows that

$$F_v > 0 \text{ if } \begin{cases} |R_I| \leq R \\ |d_I| \leq d/2 \\ |R_I| \geq R_H \end{cases} \quad (8)$$

### Thrust and torque distribution

The body force exerted on a certain cell within the propeller disk can be calculated in several ways. The most accurate representation is to model the lift and drag of the blades along radius by separating them into finite elements, each having a certain foil shape and attitude to the oncoming flow. This is known as Blade Element Momentum theory (BEMt.) Simplifications to this can be made by allowing the blades to sweep over a certain distance to give average values in larger sectors of the disk. A further step is to assume that the propeller rotates fast enough for the thrust and torque to be smeared over the entire disk at any given time step. The approach to modelling the blades depends on the amount of information is needed about the instantaneous effect of the blades on the surrounding fluid. This must be put in relation to the time scales of other phenomena around the propeller such as vortices separating from the stern area and how well the interaction of these with the propeller is to be modelled.

In this case the frequency of the waves passing and thus the variations in resistance and surge are deemed most important. The relation between the passing period of wave crests  $T_e$  at different  $\lambda/L$  in relation to different rotational frequencies  $1/T_r$  for the propeller are shown in Fig. 7. The rotational frequency is given as the full scale RPM found as  $RPM_{full} = \alpha^{-0.5} RPM_{model}$  where  $\alpha$  is taken as an example scale factor of 40 ( $L_{pp}$  of full scale ship = 120m when using the model described in Table 1.)

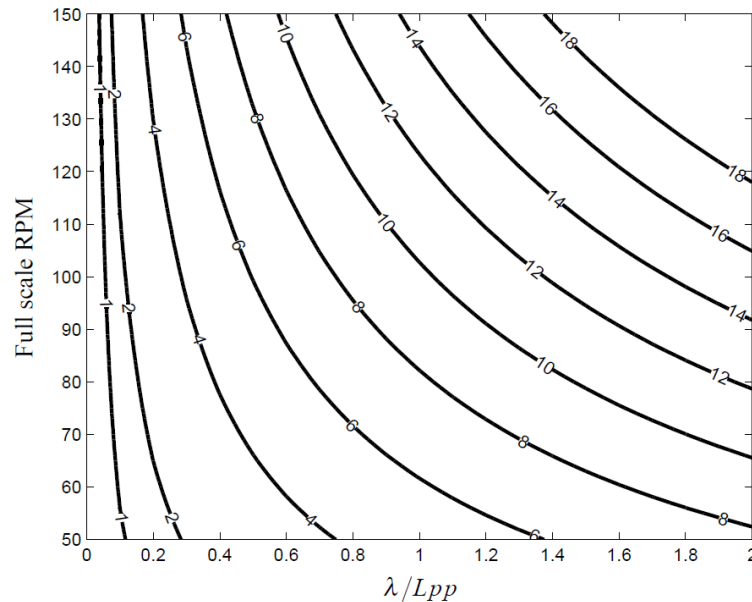


Fig. 7 Contours of the ratio  $T_e/T_r$ .

As seen in Fig. 7, there will be more than 4 rotations of the propeller for every wave encounter in most situations. For low values of  $\lambda/L$ , the wave encounter frequency is significant. However, as seen in Fig. 2, the added forces due to the waves at these wavelengths are low. This means that the motions will be low and that the main simplification made by using a smeared distribution will be to ignore the periodic variation of inflow velocity due to the waves. This is something that will be true regardless of the wavelength. For the example used in this paper of  $\lambda/L = 1$ , there will be 6-12 rotations for each wave encounter. This is considered enough for a smeared approach to be applied to the thrust and torque distributions. The thrust and torque distribution inside the propeller disk is determined by a radial shape function which is zero at the hub and tip and approximately follows the Goldstein (1929) optimum distribution. A non-dimensional radius  $r_s$  is defined as

$$r_s = \frac{|R_I| - R_H}{R - R_H} \quad (9)$$

A shape function describing the thrust distribution is given as

$$f_k = r_s \sqrt{1 - r_s} \quad (10)$$

and equally for the torque

$$f_Q = \frac{r_s \sqrt{1 - r_s}}{r_s(1 - R_H) + R_H} \quad (11)$$

The shape functions  $f_K$  and  $f_Q$  are shown in Fig. 8.

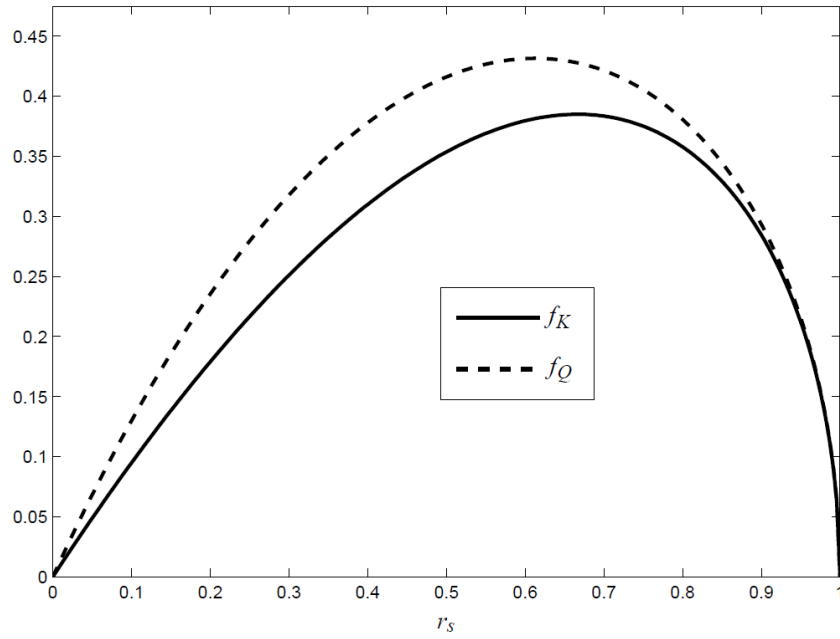


Fig. 8 Shape functions  $f_K$  and  $f_Q$ .

The shape functions are normalized so that the summation value over the entire disk corresponds to the desired thrust and torque

$$f_{KN} = F_K \frac{O f_K}{\sum V_I f_K} \quad (12)$$

$$f_{QN} = F_Q \frac{\gamma f_Q}{\sum V_I R_I f_Q} \quad (13)$$

where  $F_K$  is the thrust and  $F_Q$  is the torque.  $\gamma$  is a unit vector describing the direction of the circumferential force in each cell and is defined as

$$\gamma = \frac{O \times R_I}{|O \times R_I|} \quad (14)$$

The direction of rotation can be altered by replacing Equation 14 with



$$\gamma = \frac{-O \times R_I}{|O \times R_I|} \quad (15)$$

The body force for a cell  $I$  is now given as

$$F_{vI} = f_{KN} + f_{QN} \quad (16)$$

The thrust and torque are decided by the coefficients of thrust and torque  $K_T$  and  $K_Q$  as well as the current working RPM.

$$F_K = K_T \rho \left( \frac{RPM}{60} \right)^2 (2R)^4 \quad (17)$$

$$F_Q = K_Q \rho \left( \frac{RPM}{60} \right)^2 (2R)^5 \quad (18)$$

Since the propeller blades are not explicitly modelled in this case, the variation of  $K_T$  and  $K_Q$  with the RPM is not known. For stock propellers such as the Wageningen B-series, these can be found by interpolation of tabulated values based on experimental data for example from Bernitsas et al. (1981). Here, a 5th order polynomial fit to the open water characteristics of a MARIN 7967 propeller as described by Carrica et al. (2013) is used where

$$K_T = 0.398399 - 0.067794J - 1.286040J^2 + 2.286960J^3 - 2.039820J^4 + 0.676130J^5 \quad (19)$$

$$K_Q = 0.051144 - 0.000390J - 0.171650J^2 + 0.330060J^3 - 0.327865J^4 + 0.119477J^5 \quad (20)$$

In this case, the inflow speed is taken as the base forward speed  $U_0$  plus the velocity of the propeller centroid relative to the moving reference frame. This gives the advance coefficient  $J$  as

$$J = \frac{60 \left( U_0 + \frac{\partial xp}{\partial t} \right) \cdot O}{RPM R} \quad (21)$$

In Equation 21, care must be taken with the signs of  $U_0$  and  $\partial xp / \partial t$  so that they, with the coordinate system used, have the same definition of positive speed.

Equations 17 and 18 as well as the shape functions (Equations 10 and 11) assume that the flow into the propeller is uniform so that the local advance ratio is constant along the circumference. If the propeller is working behind a hull, the wake created by the ship will distort this condition. The thrust and torque varies periodically because of the surging motion through Equation 21. However, the presence of the waves would also mean a periodic variation of thrust and torque due to an unsteady wake, something that is not considered here. By applying a BEMt method post run-time to estimate the thrust and torque variations behind the Wigley hull in this study, Windén et al. (2013) found a thrust variation of 16% around the mean value due to the unsteady wake.

## PROPELLER CONTROL

Since the thrust produced by the propeller is a function of the RPM, it is possible vary the RPM based on given criteria for the thrust. In the interest of maintaining a constant service speed in waves, the RPM can be varied as to maintain the thrust needed to keep constant forward speed. Since the undisturbed forward speed is modelled with a current in this case, keeping constant speed is equivalent with keeping zero surge motion.

This can be achieved in two ways. The most direct approach is to iterate in each time step to find the thrust that will ensure force balance in the surge direction. The other alternative is to use a control function to steer the RPM towards the correct value based on information available from previous time steps. The second approach is preferable here, both in terms of computational time but, more importantly because it more closely represents a situation that could be applied on a real ship.

Because of the nonlinear properties of marine propulsion systems, to achieve optimal propulsion performance it is necessary to apply some sort of control algorithm to govern the propeller RPM (Xiros, 2002). This is particularly important when ship dynamics are also considered as a factor (Kashima and Takata, 2002). A similar approach as the one described in this paper with a body force propeller and PID regulator for the RPM was applied by (Carrica et al., 2008) for studying broaching events.

### PID-controller

The PID controller is defined by letting the RPM in a time step be a function of the RPM in the previous time step and a correction value based on an error  $e$ , the rate of change of the error and the integral value of the error since the start of the simulation.

$$RPM_n = RPM_{n-1} + K_p e + K_d \frac{de}{dt} + K_i \int e dt \quad (22)$$

An appropriate definition of the error  $e$  must be chosen to link the thrust from the propeller to the surge movement of the hull. Care is taken here to only include variables that could be feasibly measured on a real ship. For example, the hydrodynamic drag as well as the thrust is available in the RANS-solver and the difference between them could make up the error  $e$ . However, neither the thrust nor the resistance can be feasibly measured on board a ship in real time. For this reason, the acceleration of the centre of gravity is chosen as the main control variable. The acceleration can be measured in real time by placing an accelerometer at an arbitrary location provided the position of that location relative to the centre of gravity is known. The error  $e$  is thus based on the acceleration in the direction of travel ( $a \cdot x_1$ ).

To accentuate the connection with the resistance, the acceleration is multiplied by the mass of the ship to give an estimate of the current force acting on the hull. Furthermore, to avoid motion with constant velocity (in this case meaning that the hull moves with constant velocity other than the one specified) a penalty of 1000 is put on the integral value of acceleration. The error is now defined as

$$e = -m (a \cdot x_1) - 1000 \int (a \cdot x_1) dt \quad (23)$$

### RPM limiting

In addition to the PID-controller governing the RPM, some restrictions must be applied to make the simulation more realistic. The RPM should not be allowed to exceed a certain value since that would mean a great risk of cavitation and damage to machinery in a real propulsion system. Furthermore, large acceleration of the propeller rotation should also be disallowed since the torque needed to achieve such acceleration lies beyond the capability of both engines and propeller shafts. Furthermore, RPM increases are usually limited in marine engines to avoid large heat gradients etc. A typical maximum value for how fast the propeller rotation is allowed to change is around 1 RPM per minute in full scale. If the example scale factor of 40 is applied in this case, this is equivalent to a maximum increase of 0.67 RPM/s in model scale. Furthermore, typical working shaft-RPM for most large merchant vessels lie between 40 and 100 RPM. This corresponds to between 250 and 630 RPM in the example model scale.

## RESULTS

Simulations are started from an initialised solution where the steady wave pattern of the hull is allowed to develop. At the initial state, the resistance is recorded and the starting RPM is set as to match this resistance with a corresponding thrust. The hull is then subjected to regular waves with the first crest reaching the hull about  $t/T_e = 3$ .

Table 2 PID coefficients and initial RPM value.

$K_p$	1.2	$K_d$	0
$K_i$	0.5	Start RPM	496.4

All the information about the propeller extent and position are shown in Table 3

Table 3 Positioning and extent of propeller.

$R$	$0.0796875m$	$O_0$	$(1, 0, 0)$
$d_I$	$0.0159375m$	$xp_0$	$(1.53, -0.1078125, 0)$
$R_H$	$0.00796875m$	$CG_0$	$(0, -0.0175, 0)$

Nine different values on the maximum permissible RPM change rate  $\partial RPM / \partial t$  are tested as well as a reference case where the acceleration is unlimited. The tested constraints are listed in Table 4.

Table 4 RPM constraints.

#	max $\partial RPM / \partial t$	#	$\partial RPM / \partial t$
1	0.65	6	0.9
2	0.60	7	1
3	0.70	8	$\infty$
4	0.80	9	2
5	0.50	10	3

Controllers 2-5 performs similarly in terms of surge motion compared to controller 1, significant differences are only found for controllers 6-10. In Figs. 9, 10 and 11, the forward speed, surge and RPM for controllers 1, 7 and 10 are shown. Finally, the delivered power, which can be calculated as  $P_D = 2\pi F_Q RPM / 60$  (Molland et al., 2011) is shown in Fig. 12.

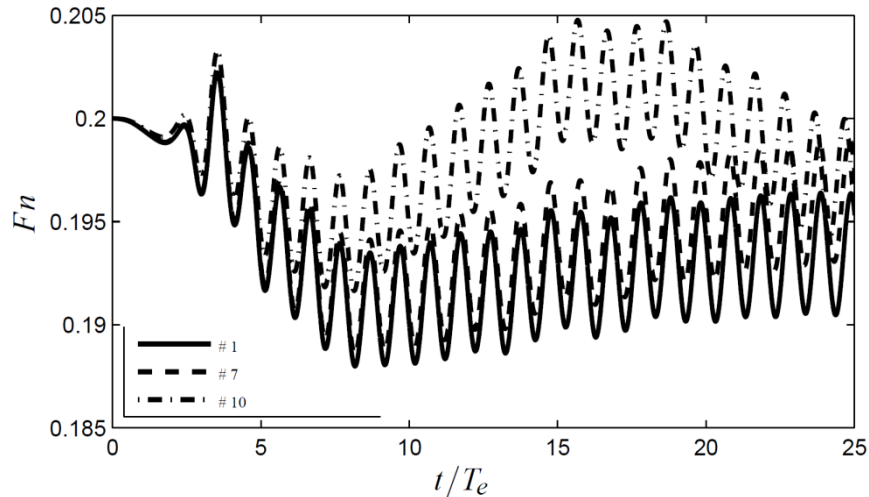


Fig. 9 Changes in forward speed due to waves with different values of  $\partial RPM / \partial t$  allowed.

As seen in Fig. 9, the hull experiences a periodical oscillation in forward speed due to the waves. There is also a drop in the mean velocity. This is due to the mean increase in resistance due to waves  $R_{AW}$ . It is clear that none of the controller constraints are generous enough to influence the periodical velocity notably. The RPM in all cases follows the maximum permitted increase. However, the higher the permitted value of  $\partial RPM / \partial t$  is, the faster the ship can overcome  $R_{AW}$  with an increased thrust and return to the original forward speed. This however comes at the cost of a higher power delivered to the propeller as seen in Fig. 12. Controller 8 is very successful in keeping constant forward speed, however the RPM increases (and subsequent power) required to do so are not in any way related to reality which is why controller 8 is excluded from the results figures.

As seen in Figure 10, even though the hull returns to its initial forward speed, the integral value of the velocity means that it has been given a large distortion in surge. While this is not a problem in real applications, in this case it means that the mesh has

been distorted. In the interest of accuracy future implementations should take this into consideration.

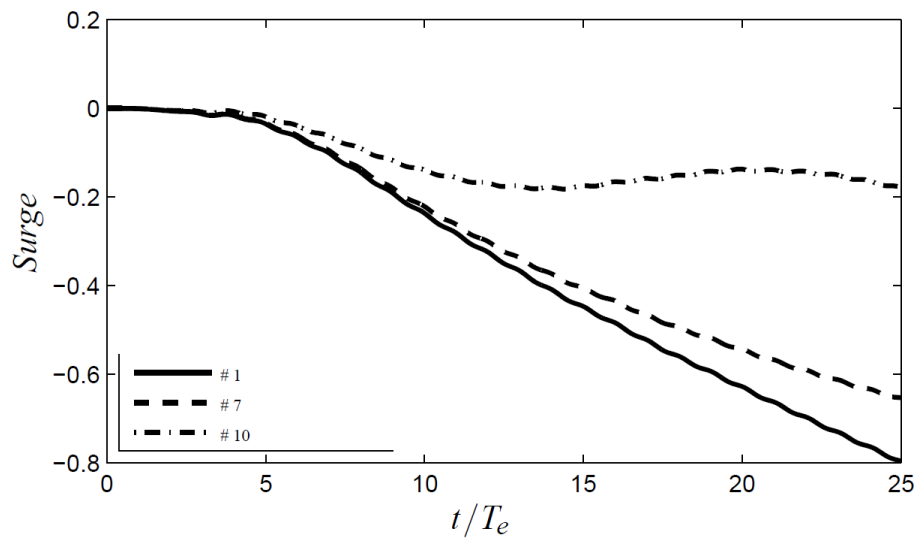


Fig. 10 Changes in surge due to waves with different values of  $\partial RPM / \partial t$  allowed.

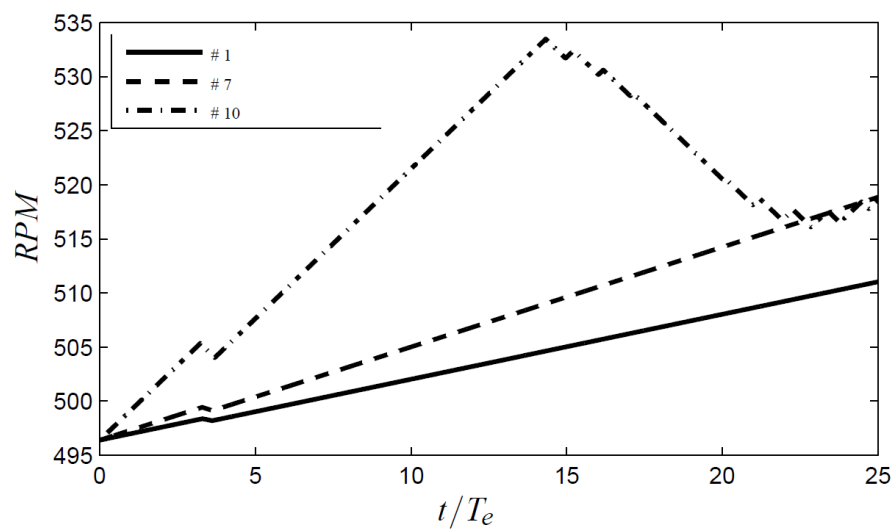


Fig. 11 Development of propeller RPM with different values of  $\partial RPM / \partial t$  allowed.

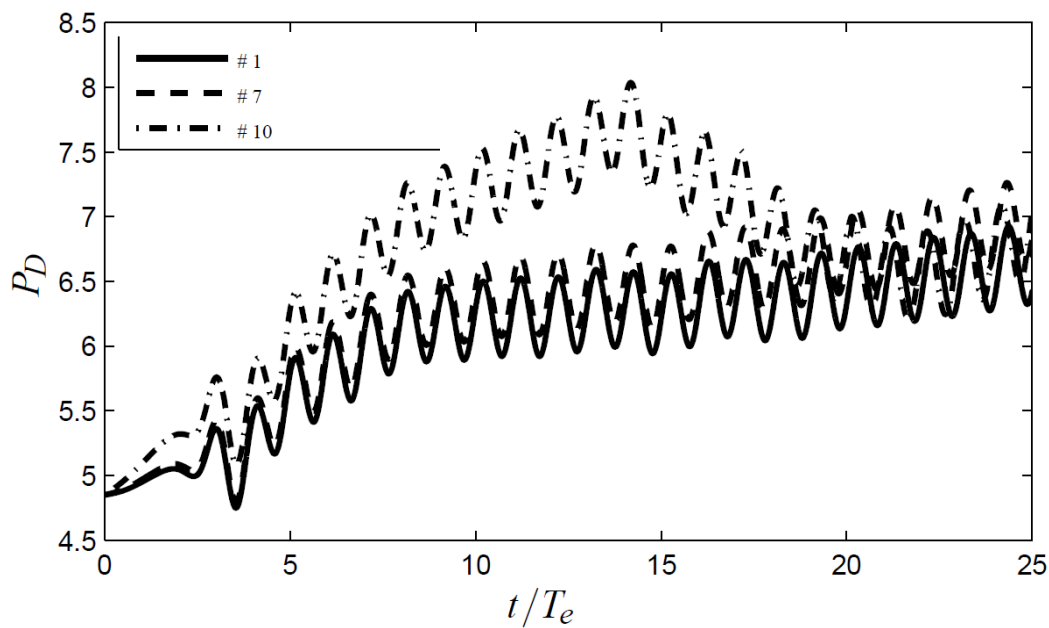


Fig. 12 Changes in delivered power with different values of  $\partial RPM / \partial t$  allowed.

If the actual powering performance in waves is sought, it would not be suitable to construct a controller that puts a penalty on the surge drift. Instead it would be preferable to initialize the simulation from a fixed hull in waves and use the RPM needed to overcome  $R_{AW}$  as the initial condition.

## CONCLUSIONS

The controller function described in this paper is a simplified version which mostly serves to demonstrate the opportunities of using open source RANS modelling with external inputs to more closely represent real operating conditions. Much more advanced controlling algorithms could be employed here, see for example Xiros (2002). Furthermore, the actuator disk model has many limitations. To properly include the propeller geometry and to draw more detailed conclusions about the effects of unsteady loading, a BEMt approach is preferred. The future aim for this model is to replace the actuator disk formulation with the BEMt model developed by Phillips et al. (2009; 2010).

This study has shown that it is possible to model and discuss around several aspects of self-propulsion using the described method. There is however need for proper validation against experimental data to ensure the accuracy of the model. The benefit of using RANS CFD to do this rather than experimental methods is that the entire flow field can be accessed and analysed to study the influence of e.g. changes in bow and stern shape and the subsequent change in performance. The future goal is to apply the methodology described in this paper to more realistic hull forms to be able to conduct detailed studies on more of the factors affecting ship performance in waves.

Finally, the conclusions drawn regarding the controller constraints may become relevant with future engine development (with for example fuel cell powered electrical engines) where the RPM increase should be able to happen faster than with current marine diesels.

## ACKNOWLEDGEMENTS

All RANS-CFD simulations conducted as a part of this paper uses the open source CFD package OpenFOAM. The research has been conducted within the framework of the research project entitled *ship design for enhanced sustainability* which is sponsored by the Lloyd's Register Educational Trust whose support is gratefully acknowledged.

## REFERENCES

- Bernitsas, M., Ray, D. and Kinley, P., 1981. Kt, Kq and efficiency curves for the Wageningen B-series propellers, Technical report. Ann Arbor: Department of Naval Architecture and Marine Engineering College, The University of Michigan.
- Carrica, P., Ismail, F., Hyman, M., Bhushan, S. and Stern, F., 2013. Turn and zigzag maneuvers of a surface combatant using a URANS approach with dynamic overset grids. *Journal of Marine Science and Technology*, **18** pp 166-181.
- Carrica, P., Paik, K., Hosseini, H. and Stern, F., 2008. URANS analysis of a broaching event in irregular quartering Seas. *Journal of Marine Science and Technology*, **13**, pp.395-407.
- Goldstein, S., 1929. On the vortex theory of screw propellers. *Proceedings of the Royal Society of London*, **123**(792), pp.440-465.
- IMO, 2011. MARPOL annex VI energy efficiency amendments, Technical report, Resolution MEPC.203(62). London
- Jacobsen, N.G., Fuhrman, D.R. and Fredsøe, J., 2012. A wave generation toolbox for the open-source CFD library: OpenFoam<sup>®</sup>. *International Journal Numerical Methods in Fluids*, **70** pp 1073-1088..
- Journée, J., 1992. Experiments and calculations on 4Wigley hull forms in head waves, Technical report, Report 0909. Delft university of Technology, Delft.
- Kashima, T. and Takata, J., 2002. An optimal control of marine propulsion system considering ship dynamics. In *Proceedings of the 2002 IEEE International Conference on Control Applications*, Glasgow, UK, September 18-20 2002, pp 1058-1063..
- Kjellberg, M., 2011. Fully nonlinear unsteady three-dimensional boundary element method for force predictions on a restrained hull in waves. Thesis for the Degree of Licentiate of Engineering. Chalmers University of Technology.
- Larsson, L., Stern, F. and Visonneau, M., 2014. Numerical ship hydrodynamics. An assessment of the Gothenburg 2010 Workshop, New York, Springer, pp 185..
- Menter, F., Kuntz, M. and Langtry, R., 2003. Ten years of industrial experience with the SST turbulence model. *Heat and Mass Transfer* 4, West Redding, Begell House Inc., pp.625-632.
- Molland, A., Turnock, S. and Hudson, D., 2011. Ship resistance and propulsion: practical estimation of ship propulsive power. New York, Cambridge University Press.
- Phillips, A., Turnock, S. and Furlong, M., 2009. Evaluation of manoeuvring coefficients of a self-propelled ship using a blade element momentum propeller model coupled to a Reynolds averaged Navier Stokes flow solver. *Ocean Engineering*, **36**(15-16), pp.1217-1225.
- Phillips, A., Turnock, S. and Furlong, M., 2010. Accurate capture of rudder-propeller interaction using a coupled blade element momentum-RANS approach. *Ship Technology Research(Schiffstechnik)*, **57**(2), pp.128-139.
- Windén, B., 2012. Powering performance of ships in waves. M.Phil/Ph.D Transfer thesis. University of Southampton.
- Windén, B., Turnock, S. and Hudson, D., 2012. Validating force calculations using OpenFOAM<sup>®</sup> on a Fixed Wigley hull in waves. In *Proceedings of the 15th Numerical Towing Tank Symposium*, Cortona, Italy, 7-9 October 2012, pp.170-175.
- Windén, B., Turnock, S. and Hudson, D., 2013. Predicting powering performance changes for ships in offshore conditions from small design modifications. In *Proceedings of the 23rd International Offshore and Polar Engineering Conference (ISOPE13)*, Anchorage, Alaska, June 30th - July 5<sup>th</sup> 2013, pp 773-780.
- Xiros, N., 2002. Robust control of diesel ship propulsion. London: Springer-Verlag.